Heliyon 10 (2024) e26728

Contents lists available at ScienceDirect

Heliyon

journal homepage: www.cell.com/heliyon

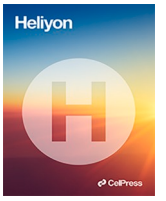

Research article

Soil erodibility mapping of hilly watershed using analytical hierarchy process and geographical information system: A case of Chittagong hill tract, Bangladesh

Rubaiya Zumara [a], N M Refat Nasher [b,*]

[a] Department of Geography and Environment, Jagannath University, Dhaka, Bangladesh
[b] Faculty of Life and Earth Sciences, Jagannath University, Dhaka, Bangladesh

ARTICLE INFO

Keywords:
Hilly watershed
Soil erosion potential
Hypsometric analysis
Analytical hierarchy process (AHP)
Geographic information systems (GIS)
Bangladesh

ABSTRACT

Soil erosion across watersheds and river basins is an alarming environmental deterioration process that poses severe risks to hydrological systems, hydrogeochemical processes, agricultural productivity, and the global natural ecosystem. The use of the Analytical Hierarchy Process (AHP) and Geographical Information System (GIS) to assess soil erosivity for the watershed is widely known. This study applied the AHP and GIS to understand the degree of erosivity of the hilly Karnaphuli watershed in Chattogram, Bangladesh. The study used topographical maps, soil maps, and satellite imagery datasets. It implemented the GIS-based AHP and weighted overlay technique to derive eight factors (slope, elevation, Stream Power Index (SPI), Land Use and Land Cover (LULC), curvature, soil, Topographic Wetness Index (TWI), and rainfall. The geological stage of erosion potential was also identified using Digital Elevation Model (DEM) data through GIS-based hypsometric analysis. The findings demonstrated that the eastern and north-western parts are particularly vulnerable to erosion compared to other parts of the study area. The most dominant variables identified to influence the process of soil erosion are slope, LULC, elevation, and SPI. According to the AHP analysis, slope was the most influential factor (26%), followed by LULC (23.8%), elevation (20.3%), and SPI (13.9%) in the soil erosion process, and the geological stage of erosion potential was determined from the hypsometric curve (S-shaped) and hypsometric integral (0.49), which revealed that moderately eroded areas characterized the whole research region. The findings are significant as they provide valuable information for researchers and planners to address soil erosion and develop measures to control it effectively.

1. Introduction

Soil erosion is a severe problem that occurs worldwide and has a wide range of negative consequences in addition to the unavoidable off-site effects such as silt accumulation, eutrophication of watercourses, and the rise in the severity of floods. These include land degradation and soil fertility loss [1,2]. The power of water or wind disperses the soil particles, which might get eroded when carried and dumped elsewhere. Additionally, erosion happens when soil aggregates are broken apart by irrigation or precipitation [3]. In agriculture, the process of topsoil loss brought on by water agents is referred to as soil erosion. This widespread issue affects distinct regional landforms [4]. Water flow-induced erosion is a natural occurrence that affects the ecosystem and the soil's biological,

* Corresponding author.
E-mail address: refat@geography.jnu.ac.bd (N.M.R. Nasher).

https://doi.org/10.1016/j.heliyon.2024.e26728
Received 7 July 2023; Received in revised form 17 February 2024; Accepted 19 February 2024
Available online 22 February 2024

physical, and chemical characteristics. It depletes soil fertility, contaminates streams, and overflows reservoirs [5]. Soil erosion is a significant ecological concern with global implications due to the depletion of nutrients and other essential supplements found in topsoil [6]. Asia exhibits a significantly high erosion rate, averaging 74 tons per acre annually, positioning it among the regions with Earth's most pronounced erosion levels [7].

In basin studies, boundaries, drainage systems, and morphometric features may be extracted using various methods and methodologies. Though some investigators use traditional procedures to assist their investigations, such as topographical maps and field surveys, others favor more contemporary approaches, such as remote sensing techniques, digital surface models (DSMs) created by GIS, and DEMs and digital surface models (DSMs) [8,9]. Because of availability and simplicity of operation, satellite-based DEMs are now widely used in such studies. The Advanced Space-borne Thermal Emission and Reflection Radiometer (ASTER), the SRTM with 90 m and 30 m, the Advanced Land Observing Satellite (ALOS), and the Panchromatic Remote-sensing Instrument for Stereo Mapping (PRISM) −30 m have all enhanced resolutions that are now freely available. Therefore, Digital Elevation Models (DEM) and Digital Surface Models (DSM) are advanced techniques that precisely calculate characteristics. The utilization of GIS and image processing techniques enables the identification and characterization of the basin's physical attributes and drainage patterns.

Consequently, the application of remote sensing data in this context proves significantly advantageous [10]. The inhabitants living in erosion-prone locations are significantly impacted by Bangladesh's dynamic river morphology and unexpected erosion processes [11]. The fluctuations of the river flow pattern and slope variability in mountainous areas cause the loss of soil structure, which leads to soil erosion naturally in Bangladesh's river basins. Aside from dry, semi-humid, and semi-arid regions, rivers that start in mountainous regions are particularly vulnerable to soil erosion [12,13]. The Karnaphuli River, which originates in the Lushai highlands of the Indian state of Mizoram, is the principal river in the Chattogram district of Bangladesh. Due to its immense ecological and economic significance, it is known as the "Life Line Chattogram" and finally joins the Bay of Bengal near the Chattogram seaport. The river is around 116 km long and through the southeastern part of Bangladesh [14]. It has around 100 tributaries, of which two-thirds are in Bangladesh, and the River Karnaphuli's downstream exhibits typical estuarine features [15]. The downstream portion of the river Karnaphuli has typical estuarine characteristics. The river has a significant role in the Kaptai Hydroelectric Power Plant and Bangladesh's economy.

This study aims to create and evaluate a multi-criteria integrated strategy for erosivity mapping using AHP, encompassing data from spatial analysis using GIS and statistical analysis. This study was also carried out to assess the erosion status of the Karnaphuli River basin by analyzing morphometric and topographic characteristics of the watershed that can be useful to understand the morphological changes and denudational processes and help to take soil and water protection measures. In basin morphometric research, DEMs have frequently been employed. The ability of DEMs to display surface topographical features depends on their spatial resolution [16]. Obtaining high-resolution digital elevation models (DEMs) allows for a more extensive collection of topographic data, offering greater detail and comprehensive information [17]. The literature review shows that the previous study was carried out to assess the causes of erosion, its impacts on local communities, and mitigation strategies for erosion and soil pollution problems in the study area of Bangladesh [18–21]. The current study tried to obtain the following specific objectives to fill these gaps.

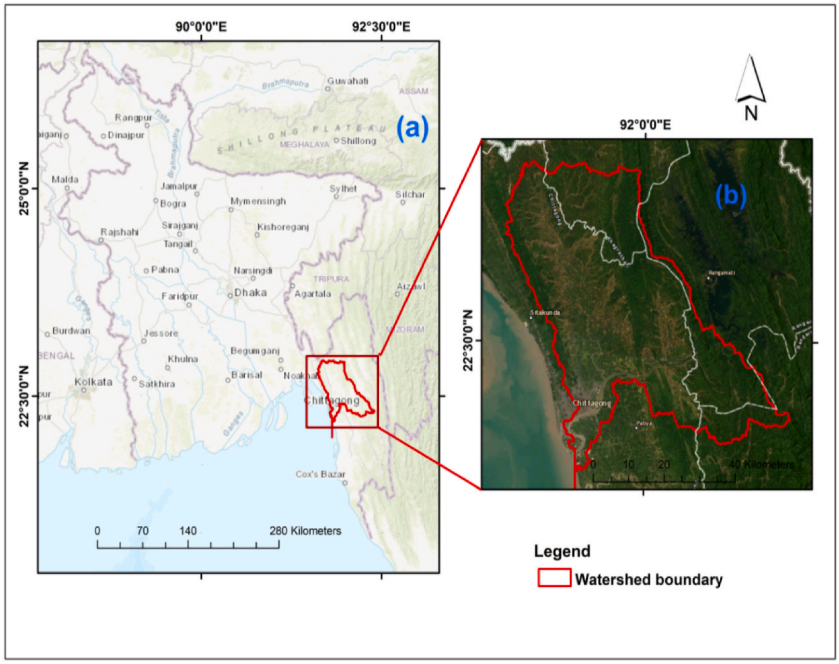

Fig. 1. a) Study area on Bangladesh map, b) Location of Karnaphuli Watershed.

1. to explore the stage of geomorphic evolution and geological development of the Karnaphuli Watershed through hypsometric analysis,
2. to assess the erosion potentiality of the Karnaphuli Watershed and
3. To identify the areas vulnerable to soil erosion using AHP.

2. Study area

In the Chattogram hill tracts, the Karnaphuli River is one of the largest and most significant rivers. The river has a catchment area of around 11,000 sq. km and rises in the Lushai Hills of Mizoram, India [22]. At Rangamati in Bangladesh, the river runs over 180 km of hilly wilderness before passing through Chattogram, a port city, for about 170 km and then empties into the Bay of Bengal. Geologically, the entire river basin comprises tertiary rocks that serve as a substratum for alluvial deposits coated in mud and sand layers [23]. One of the most significant estuaries in Bangladesh is the Karnaphuli River Estuary, which lies close to Patenga in Chattogram City between latitude 22°53′ and longitude 91°47′E. Semidiurnal tides characterize the estuary with a 2–4 m variation and an average 8–10 m channel depth in the exterior zone [24]. Environmental characteristics in the Karnaphuli estuary change periodically due to the strong effect of the Indian monsoon [25]. The given Fig. 1(a and b) shows the study area.

3. Materials and methods

3.1. Data collection and processing

Planning and investigating the effects of numerous erosion-causing factors is necessary to predict soil erosion susceptibility [26] effectively. Different types and sources of data, including soil data, digital elevation models, and satellite data, were employed in the current study. The fundamental datasets utilized are the Shuttle Radar Topographic Mission (SRTM) Digital Elevation Model (DEM) and satellite images from the USGS Earth Explorer data portal, accessed on February 15, 2023 (https://earthexplorer.usgs.gov). Data on land cover (ESA Sentinel-2 imagery at 10 m resolution) was acquired on the same date from the Esri Sentinel-2 Land Cover Explorer website. The study area was extracted from these datasets of the FAO Digital Soil Map of the World (DSMW).

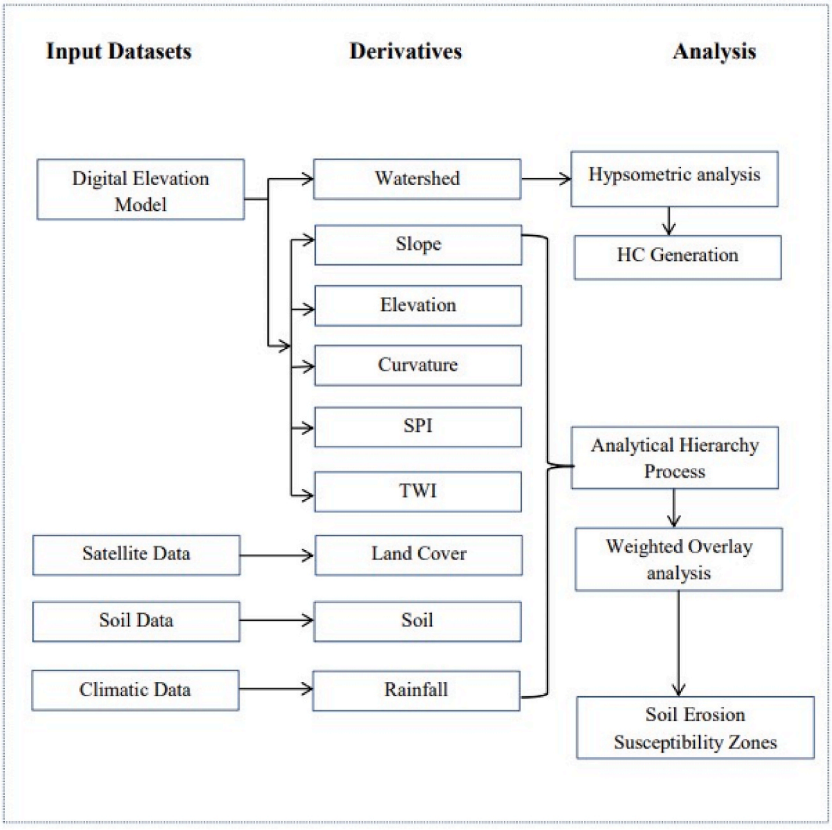

Fig. 2. Soil Erosion susceptibility assessment flowchart.

3.2. Preparing the thematic maps

Fig. 2 shows the flowchart of making the soil erosivity map. The layout of slope, curvature, and elevation map thematic layers in GIS has been done using the natural break approach. A thematic layer of a land cover and soil map was created using Esri Sentinel-2 Land Cover and FAO-published soil data for this research. The STRM-based DEM was used to create TWI and SPI maps using ArcSWAT and Hydrology tools (Table 1).

3.3. Determination of weights by the AHP procedure

AHP analysis consists of three steps.

- identification of a hierarchy of objectives, criteria, and alternatives
- pairwise comparison of criteria
- integration with the result from pairwise comparison as relative importance in overall hierarchy levels

This strategy begins by assimilating the decomposition of decision-making concerns into a series of significant criteria and options. AHP assigns preference ratings based on the relative weight of each component to determine relative relevance concerning the target [35]. The following phase, which is comparably a superior method for assessing priorities from an uncertain pairwise evaluation matrix, specifies the weights assigned to each factor's priorities by the construction of a normalized eigenvector. To help determine weights, the sum of the values in each column of the pairwise comparison matrix is divided by the sum of the values in the constant factors' factors' column. The mean value of each row makes up the matrix's principal eigenvector. When this network is organized randomly, there may be some degree of irregularity [36]. The crucial parameters with their intensities are shown in Table 2.

The pairwise parameter in Table 2 was assigned a scale. To ensure the reliability of the assessment in this study, the consistency of the findings was evaluated and confirmed using the consistency ratio (CR) (Equation (1)) and consistency index (CI) (Equation (2) &3) [37]. These measures assess the level of consistency in the obtained results.

$$\mathrm{CR} = \frac{CI}{RI} \times 100\%, \tag{1}$$

$$\mathrm{CI} = \frac{\lambda_{\max} - \mathrm{n}}{\mathrm{n} - 1}, \tag{2}$$

$$\lambda_{\max} = \sum_{\mathrm{i}=1}^{\mathrm{n}} \mathrm{X}_{\mathrm{i,j}} \times \mathrm{W}_{\mathrm{i,j}}, \tag{3}$$

The consistency ratio's value determines a variable's inclusion or exclusion from research. It is recommended that CR's numerical value not exceed 0.1 [38]. It should fall within the range of 0.1 or less. The output parameter (CI) displays how consistently one's judgment holds up. In this case, the largest eigenvalue is "λmax," and "n" denotes the matrix's order [39]. The RI, Pairwise comparison matrix and weights of multi criteria are given in Tables 3 and 4.

Table 1
Parameters, Sources, techniques, and references used to create thematic maps.

Parameters	Source	Techniques	References
Slope	SRTM DEM https://earthexplorer.usgs.gov/	Tan θ $\frac{N \times i}{636.6}$ N = no of contour cutting; i = contour interval	[27]
Elevation	SRTM DEM https://earthexplorer.usgs.gov/	30 m × 30 m digital elevation model	[28]
Land use/land cover	Sentinel-2 10 m Land Use/Land Cover https://livingatlas.arcgis.com/landcoverexplorer/	Maximum likelihood	[29]
SPI	SRTM DEM https://earthexplorer.usgs.gov/	SPI = (A_S × tan β) A_S = specific catchment area (m^2/m), β = slope gradient (°).	[30]
Curvature	SRTM DEM https://earthexplorer.usgs.gov/	K = $\left\|\frac{dT}{ds}\right\|$	[31]
Soil	FAO Digital Soil Map of the World (DSMW) https://www.fao.org/soils-portal/data	Proximity analysis	[32]
TWI	SRTM DEM https://earthexplorer.usgs.gov/	TWI = $\frac{\alpha}{tan\,\beta}$ α = local upslope area; tanβ = local slope	[33]
Rainfall	NASA POWER Data Access Viewer https://power.larc.nasa.gov/data-access-viewer/	IDW Interpolation	[34]

Table 2
The continuous rating scale for AHP evaluation [37].

Intensity of importance	Definition	Explanation
1	Equal importance	The objective is equally controlled by two variables.
3	Somewhat more important	One variable is slightly preferred than the other
5	Much more important	One variable is very highly preferred over the other.
7	Very much more important	Very highly significance over other in practice.
9	Absolutely more important	The strongest potential validity may be found in the evidence supporting one over the other
2,4,6,8	Intermediate values	When a deal must be made.

3.4. Morphometric analysis of Karnaphuli Watershed

For morphometric analysis, hypsometric curve plotting and hypsometric integral estimation are crucial indications of watershed conditions [40]. Differences in the hypsometric curve and integral values correlate with the magnitude of instabilities in the equilibrium of erosive and tectonic forces [41]. The geologic phases of watershed development are categorized by the geomorphological quantity known as the hypsometric integral. It is crucial for determining the level of erosion in a watershed and, as a result, aids in prioritizing watersheds when suggesting actions to save soil and water. In addition, the hypsometric integral shows the 'cycle of erosion' [42,43]. The time needed to decrease a land area to its base level—the lowest point streams might take if all other variables remained constant but time—is known as the "cycle of erosion." This entire "cycle of erosion" can be broken down into three stages: (i) the fully stabilized watershed, or monadnock (old) (Hsi 0.3); (ii) the equilibrium or mature stage (Hsi 0.3 to Hsi 0.6); and (iii) the in equilibrium or young stage (Hsi >0.6), during which the watershed is exceptionally susceptible to erosion [43]. The residual landmass volume for the whole basin is related to the dimensionless hypsometric integral [44].

The hypsometric study focuses on the link between the elevation of watersheds in the dimensionless form and its horizontal cross-sectional area. Digital contour maps were employed to generate the information for relative area and elevation analyses. In order to create the hypsometric curve, the relative elevation (h/H) along the ordinate was plotted against the relative area (a/A) along the abscissa.

Using the Elevation-Relief Ratio (E) Relationship, the Pike and Wilson (1971) elevation-relief ratio approach was applied. The relationship is expressed as (Equation (4))

$$\mathbf{E} \sim \mathbf{H}_{is} = (Ele\mathbf{v}_{mean}\text{-}Ele\mathbf{v}_{\mathbf{min}}) \,/\, (Ele\mathbf{v}_{\mathbf{max}}\text{-}Ele\mathbf{v}_{\mathbf{min}}) \tag{4}$$

Where E is the elevation-relief ratio, which is equal to the hypsometric integral H_{is}; $Elev_{mean}$ is the weighted mean elevation of the watershed determined from the recognisable contours of the defined sub-watersheds; and $Elev_{min}$ and $Elev_{max}$ are the minimum and maximum elevations inside the watershed.

4. Results

Results of this research are described in terms of the following sub-headings: hypsometric Curve and integral, description of input parameters/soil erosion influencing parameters, multi-criteria contribution to soil erosion susceptibility and pairwise comparison matrix.

4.1. Hypsometric curve and integral

By using the Soil and Water Assessment Tool (SWAT) in an ArcGIS environment, it was possible to estimate the indirect state of erosion throughout the Karnaphuli watershed based on hypsometric integral value. The final calculation was completed in an Excel sheet to provide the HI value and HC curve. Table 5 shows the Hypsometric integral value and geological stage of the study area.

The investigation revealed that the watershed's HI value (0.49) indicated that the basin was mature and that the HC was an S-shaped curve (Fig. 3), indicating that moderately eroded areas characterized the study region.

4.2. Description of input parameters/soil erosion influencing parameters

A Digital Elevation Model (DEM) represents the Earth's bare ground (bare Earth) topographic surface, excluding trees, buildings, and any other surface objects. DEMs are created from a variety of sources. USGS DEMs used to be derived primarily from topographic maps. Slope, elevation, curvature, stream power index (SPI), and topographic wetness index (TWI) are the extracted parameters from DEMs used in this study.

Table 3
Random Index (RI) values for the corresponding number of criteria/alternatives.

Size	1	2	3	4	5	6	7	8	9	10
RI	0.00	0.00	0.58	0.90	1.12	1.24	1.32	1.41	1.45	1.49

Table 4
Pairwise comparison matrix.

Factors	Slope	Elevation	LULC	SPI	Curvature	Soil	TWI	Rainfall	Weights
Slope	1	1	2	3	4	5	9	7	0.255
Elevation	1	1	1	2	4	3	7	9	0.206
LULC	0.5	1	1	3	5	7	8	9	0.231
SPI	0.33	0.5	0.33	1	3	5	7	9	0.141
Curvature	0.25	0.25	0.2	0.33	1	3	3	5	0.071
Soil	0.2	0.33	0.14	0.2	0.33	1	3	5	0.053
TWI	0.11	0.14	0.12	0.14	0.33	0.33	1	1	0.022
Rainfall	0.14	0.11	0.11	0.11	0.2	0.2	1	1	0.021

Consistency Ratio (C.R) = 0.54.

Table 5
Hypsometric integral value and geological stage.

Watershed	Area in Sq. Km.	Slope(^{O})			Elevation(m)			Hypsometric integral (HI)	Geological stage
		Maximum	Minimum	Mean	Maximum	Minimum	Mean	0.49	Mature
Karnaphuli	3058.33	67.92416	0	12.446	546	−37	240.581		

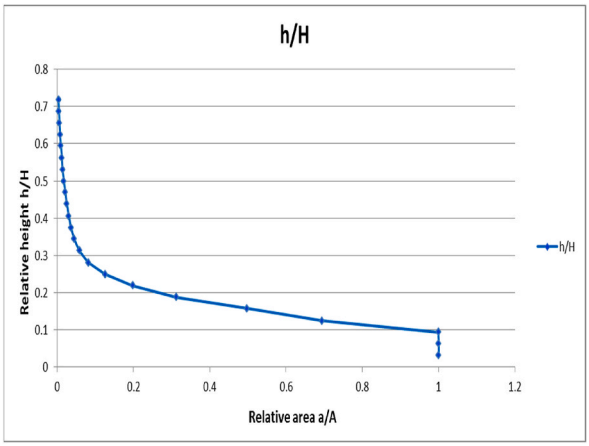

Fig. 3. Hiposometric curve of Karnaphuli watershed.

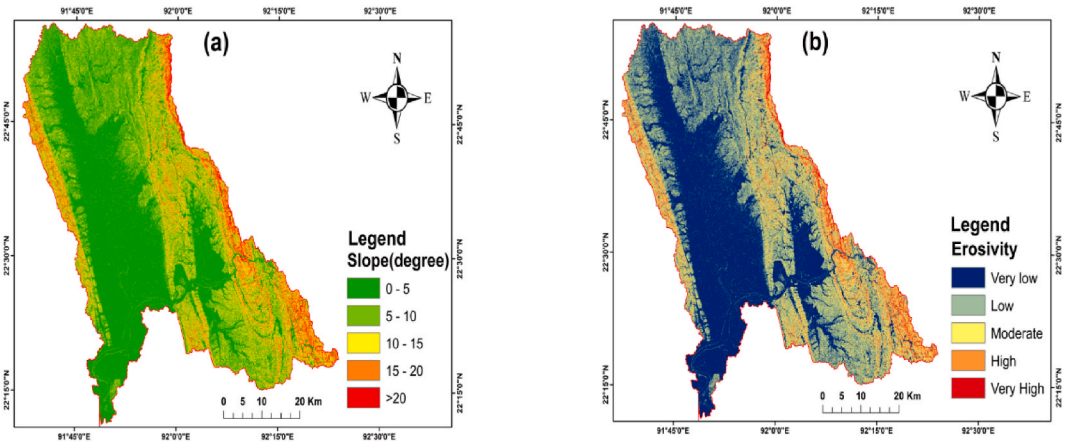

Fig. 4. a) Slope map, b) Reclassified Slope map.

4.2.1. Slope map

A critical factor in preventing erosion is the slope gradient. Steeper slopes are more likely to experience soil erosion, a well-known phenomenon [45]. The steeper slope accelerates the flow of the surface, causing more soil erosion [46]. The contour cross-section and contour break calculated the slope factor. The slope's steepness and length influence both runoff and soil erosion. The slope's form is another aspect of the slope that influences erosion. The digital elevation model (DEM) in raster format was utilized to generate the slope map by applying the Hydrology tool of ArcGIS 10.5 version. The slope class map was given, as shown in Table 5 and Fig. 4a and b, indicating its propensity for soil erosion.

4.2.2. Elevation map

The rate of erosion is significantly influenced by elevation due to its impact on various factors such as soil moisture, water balance, erosional and depositional processes, soil organic matter, biomass, and the production of cultivated crops and natural vegetation [4]. After being categorized, the elevation layer derived from the SRTM DEM was used in the overlay analysis to map locations susceptible to soil erosion in the study basin (Fig. 5a and b).

4.2.3. Land use land cover map

The geological stability of the slope is significantly impacted by land cover, which causes erosion [47] distinct land coverings exhibit distinct tendencies toward erosion depending on the size and pattern of the area covered. In this investigation, Esri Sentinel-2 Land Cover statistics were employed. That dataset was retrieved on February 15, 2023, and created using 10 m resolution ESA Sentinel-2 images. The most significant land cover types were divided into five groups based on the specific cover type: dense vegetation/natural forest, cropland, grassland, built-up area, and water bodies. The five categories of land cover types were categorized based on the vulnerability of each land use to soil erosion and the kind of each land use. Fig. 6 shows that LC consists of crops in the sloping valley, barren regions, grassland, natural trees, thick vegetation, built-up areas, and water bodies (Fig. 6a and b). Much land has high slope gradients, which significantly adds to erosion. The AHP approach also shows that soil erosion is affected by the combination of land use with elevation, slope, or curvature.

4.2.4. Stream power index (SPI) map

The SPI, which represents the erosive strength of the flowing water by assuming that the discharge is proportionate to the particular catchment area and slope, was another aspect taken into account to map regions prone to soil erosion in the watershed [24,28]. The stream power index (SPI) assessment is crucial for assessing the potential of a soil erosion location. Erosion might be brought on by overland flow [30,48]. The high SPI potentiality indicates the high energy of overland flow, which caused sediment entertainment, resulting in a higher degree of soil erosion [15]. The SPI is a metric used to quantify the erosion caused by hill downflow, supposing that discharge is proportionate to the particular catchment area [49]. According to their vulnerability to erosion, the five SPI groups were classified in Fig. 7a and b. According to researchers' and experts' expertise, the more excellent range of SPI has been given priority over the lower range of SPI when it comes to soil erosion. The empirical Equation (5) for SPI is given below;

$$SPI = (A_S \times \tan \beta) \tag{5}$$

Here.Where, A_S = specific catchment area (m^2/m), β = slope gradient (°).

4.2.5. Curvature map

The degree to which a curve strays from a straight line is called its curvature. It affects the convergence and divergence processes that result in the slope's downward flow [50]. The curvature of hillslope processes can significantly influence watershed form and

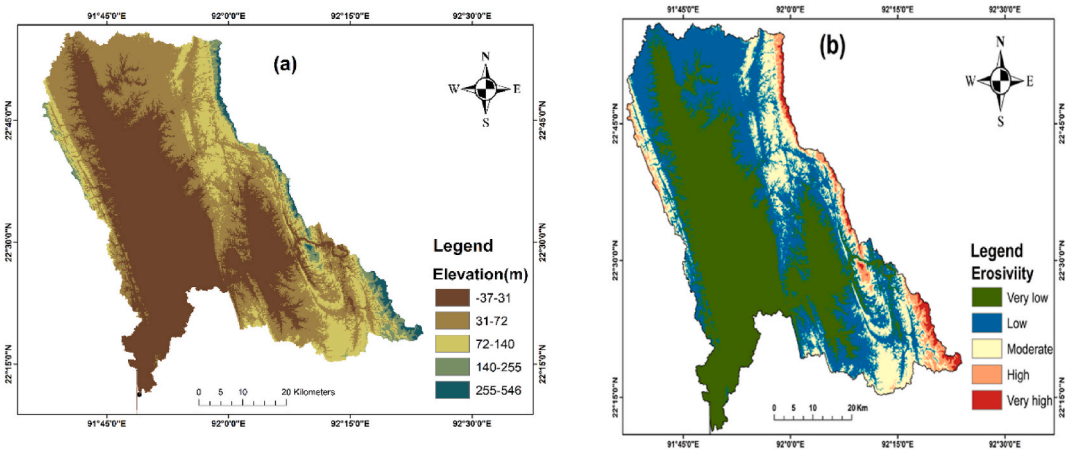

Fig. 5. a) Elevation map, b) Reclassified elevation map.

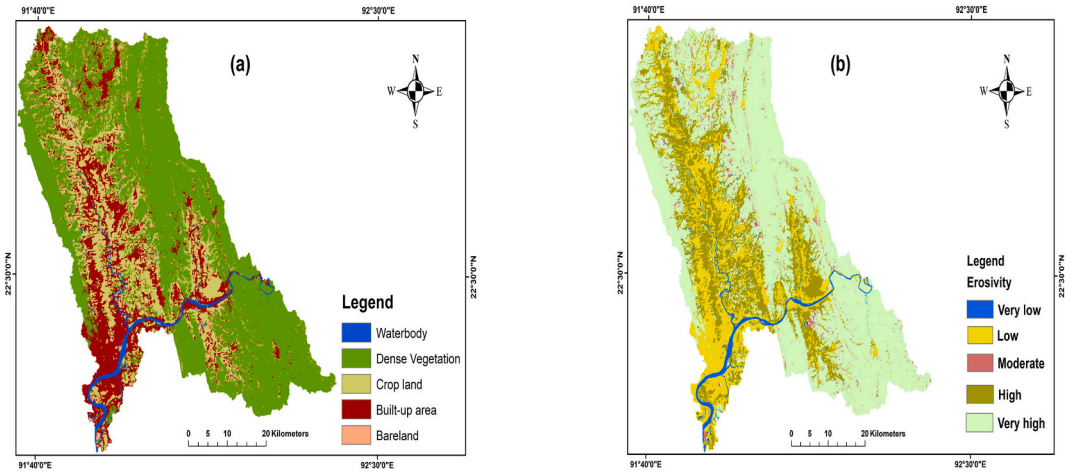

Fig. 6. a) LULC map, b) Reclassified LULC map.

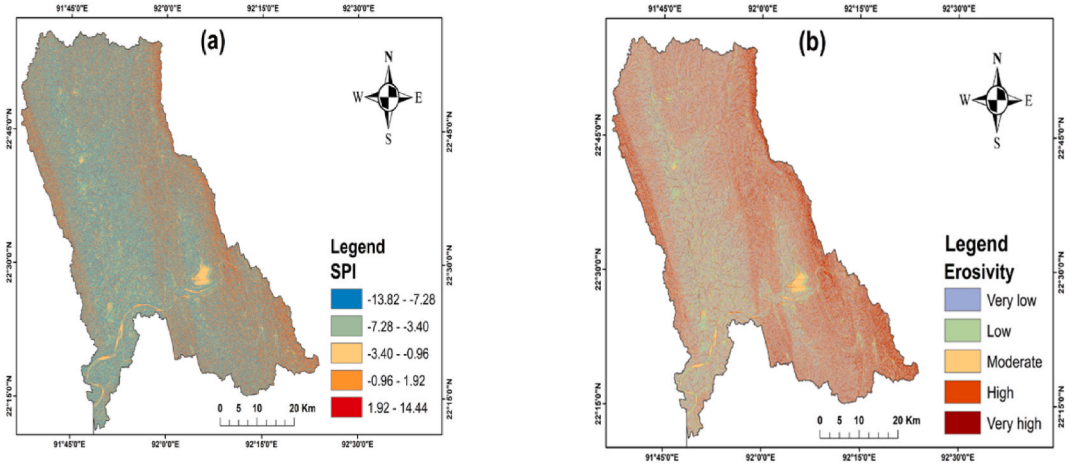

Fig. 7. a) SPI map, b) Reclassified SPI map.

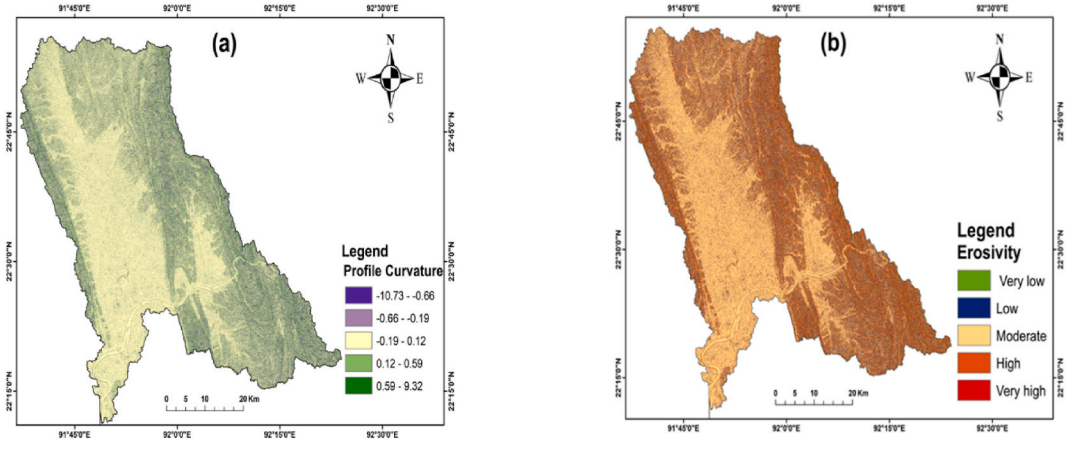

Fig. 8. a) Curvature map b) Reclassified curvature map.

Table 6
Multi-criteria contribution to soil erosion susceptibility.

Soil Erosion Susceptibility Class	Area Coverage (km^2) and Percentage (%)															
	Slope		Elevation		LULC		SPI		Curvature		Soil		TWI		Rainfall	
	km^2	%	km^2	%	km^2	%	km^2	%	km^2	%	km^2	%	km^2	%	km^2	%
Very low	1491.15	48.76	2550.13	83.38	66.83	2.19	1146.93	37.50	116.08	3.79	–		1585.85	51.85	63.568451	2.08
Low	786.80	25.73	429.46	14.04	524.85	17.16	323.33	10.57	517.68	16.93	825.55	1042.18	1042.18	34.08	361.727635	11.83
Moderate	492.29	16.09	56.76	1.86	68.36	2.24	849.09	27.76	1521.62	49.75	36.35	387.21	387.21	12.66	788.944994	25.80
High	228.23	7.46	20.0	0.66	609.40	19.93	596.51	19.51	733.29	23.98	2176	37.88	37.88	1.24	1393.26	45.56
Very high	59.86	1.96	1.98	0.07	1788.12	58.48	142.47	4.66	169.66	5.55	–		5.21	0.17	450.71	14.73

stream density. The grade of the hill slope, plan curvature, and profile curvature affect the landform features' susceptibility to erosion. The curvature of the research area is depicted in Fig. 8a and b and ranges from low (−13.82) to high (+14.44). Water impacts the surface with great force in highly curved sections, accelerating erosion [48]. Low, medium, and high curvatures are present in the research region and influence the rate of soil erosion.

4.2.6. Soil factor map

The characteristics of soil are also considered significant contributors to soil erosion. The soil types influence the land management and land use techniques in a particular location. The physical and chemical properties of soil directly influence soil erosion susceptibility [51]. The soil layer was collected and converted to raster format from the FAO global soil map, where our research region is located. Based on the physical qualities of the soil (texture and structure) presented in Table 8 and erosion sensitivity traits, the sensitivity of the soil to erosion was determined (Table 6). In the research region, there were three main types of soil. These significant soil types were classed according to their susceptibility to soil erosion (Fig. 9a and b).

4.2.7. Topographic wetness index (TWI) map

The TWI, also known as the compound topographic index (CTI), was an essential factor considered for mapping erosion hotspot locations. This variable is a proxy for soil moisture conditions in the catchment, including soil moisture content, water accumulation, and soil moisture content [52]. It explains the impacts of topography, mapping drainage, soil type, soil infiltration, crop or plant distribution, and soil's chemical and physical qualities. It is also helpful for distributed hydrological modeling. Additionally, it is crucial for planning and managing land use [53], managing watersheds, and evaluating soil and land for sustainable usage [54]. The formula was used to extract TWI from the DEM and compute it by Beven and Kirkby (1979). Higher TWI values correspond to watershed depressions, while lower values correspond to crests and ridges. The TWI map of the study area showed in Fig. 10a and b.

4.2.8. Rainfall map

Rainfall is a crucial determinant in soil erosion since it is responsible for raindrops' impact and ability to transport soil particles

Table 7
Scale value assigned to different thematic layers as per the soil erosion severity.

Sl. No.	Thematic layers	Classes	Scale value	Soil severity
1	Slope(°)	0–5	1	Very low
		5–10	2	Low
		10–15	3	Moderate
		15–20	4	High
		>20	5	Very high
2	Elevation(m)	−37–31	1	Very low
		31–72	2	Low
		72–140	3	Moderate
		140–255	4	High
		255–546	5	Very high
3	LULC	Water-bodies	1	Very low
		Built-up area	2	Low
		Bare land	3	Moderate
		Crop land	4	High
		Dense Vegetation	5	Very high
4	SPI	−13.82–−7.28	1	Very low
		−7.28–−3.40	2	Low
		−3.40–−0.96	3	Moderate
		−0.96–1.92	4	High
		1.92–14.44	5	Very high
5	Curvature	−10.73–−0.66	1	Very low
		−0.66–−0.19	2	Low
		−0.19–0.12	3	Moderate
		0.12–0.59	4	High
		0.59–9.32	5	Very high
6	Soil	Ge-Eutric Gleysols	2	Low
		Af-Ferric Acrisols	3	Moderate
		Bd- Dystric Cambisols	4	High
7	TWI	2.47–6.33	1	Very low
		6.33–8.49	2	Low
		8.49–11.09	3	Moderate
		11.09–14.68	4	High
		14.68–25.36	5	Very high
8	Rainfall	4208.59–4277.59	1	Very low
		4277.59–4346.59	2	Low
		4346.59–4415.59	3	Moderate
		4415.59–4484.59	4	High
		4484.59–4553.59	5	Very high

Table 8
Soil properties using for erosion simulation.

Soil unit symbol	sand % topsoil (m_S)	silt % topsoil (m_{silt})	clay % topsoil (m_c)	OC % topsoil (org)	f_{csand}	f_{cl_si}	f_{orgc}	f_{hisand}	*K* factor
AF	61.7	14.4	23.9	0.91	0.200	0.746	0.994	0.990	0.147
BD	32.7	30.3	37.1	3.28	0.201	0.787	0.974	1.000	0.154
GE	42.8	20.4	36.8	1.3	0.200	0.734	0.985	1.000	0.1451

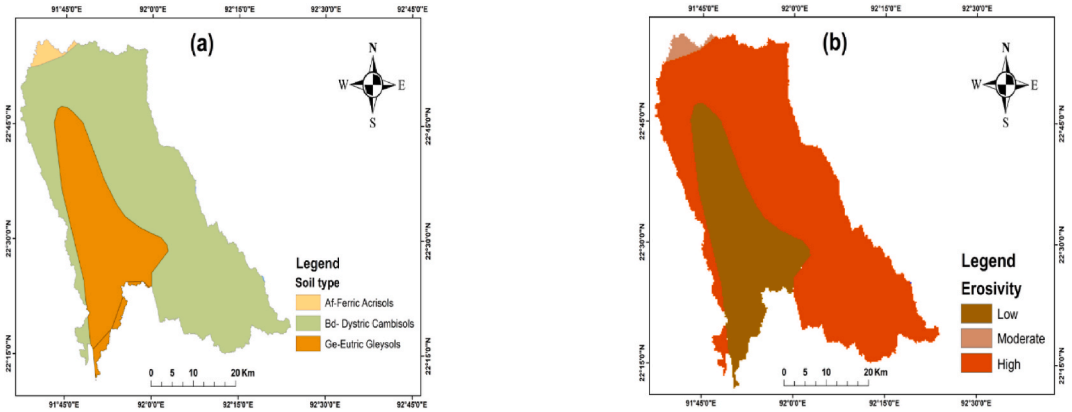

Fig. 9. a) Soil map, b) Reclassified soil map.

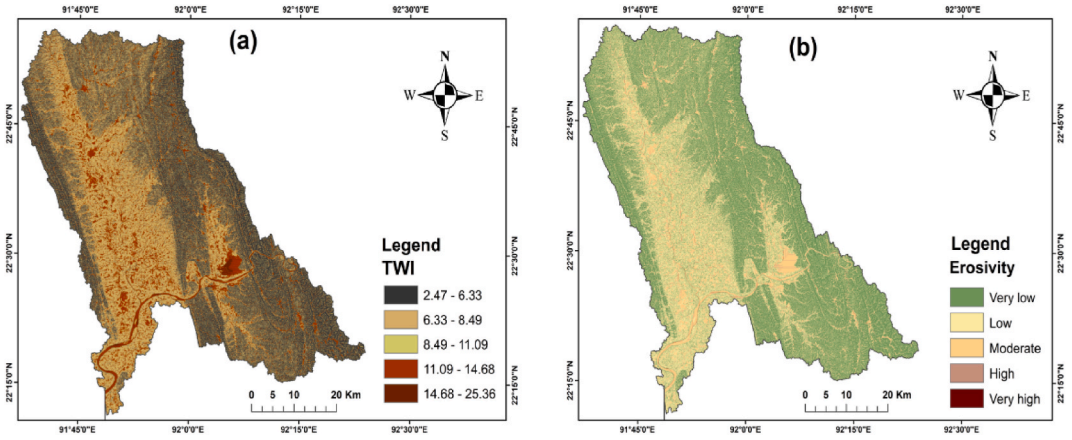

Fig. 10. a) TWI map, b) Reclassified TWI map.

downslope [55]. The rainfall data for the years (2021–2022) was collected from the NASA POWER Data Access viewer. In this research, the rainfall map (Fig. 11a and b) has been produced using the IDW interpolation method in the ArcGIS environment.

5. Discussions

This research is described in terms of the following sub-headings: soil erosion susceptibility (SES); impact of slope, elevation, LULC, SPI, Curvature, Soil, TWI, and rainfall; mapping of soil erosion susceptibility (SES) and validation of potential soil erosion risk. The assigned scale values were presented in Table 7.

5.1. Soil erosion susceptibility (SES)

As previously indicated, pairwise comparisons are made in AHP before the standard AHP technique is used to determine the relative weights for each element, as shown in Table 4. Local expertise in the subject area and the body of published literature served as the foundation for the pairwise rankings. Equation (6) produced the results that are shown below for the pixel-based soil erosion severity calculation;

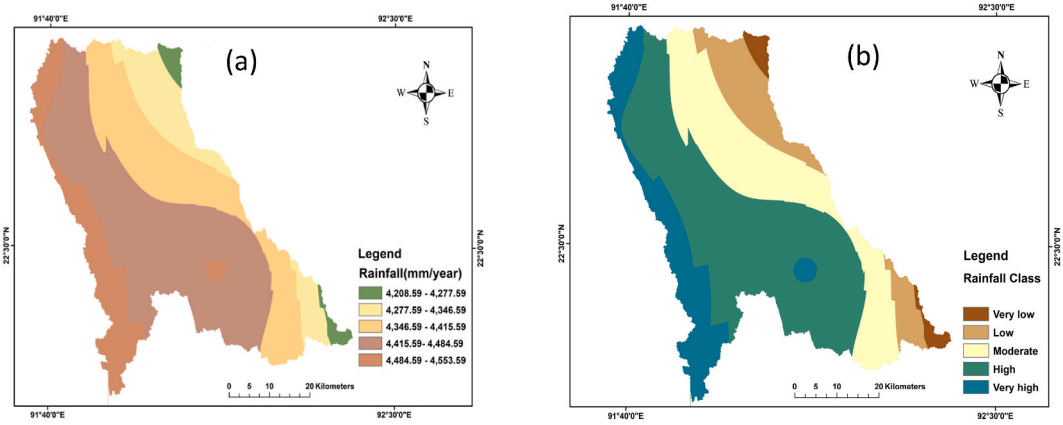

Fig. 11. (a)Annual Rainfall map and, (b) Reclassified rainfall intensity map.

$$\mathbf{SES} = \text{Slope} \times 0.302028748 + \text{Elevation} \times 0.186124204 + \text{Curvature} \times 0.092651871 + \text{LULC} \times 0.169100866 + \text{Soil} \times 0.090463053 + \text{Rainfall} \times 0.027063267 + \text{SPI} \times 0.104360057 + \text{TWI} \times 0.028207932 \quad (6)$$

5.2. Impact of slope on erosion

The slope gradient is one of the most important aspects that affect soil erosion on the Earth's surface, as was previously discussed in this study. According to the reclassified slope map (Fig. 4b; Table 6), soil erosion is a problem in 59.86 km^2 (1.96%) of the land use, 228.23 km^2 (7.46%) of the land use, 492.29 km^2 (16.09%) of the land use, 786.80 km^2 (25.73%) of the land use, and 1491.15 km^2 (48.76%) of the land use.

5.3. Impact of elevation on erosion

An further factor that affects how plants are distributed and how their morphology, physiology, and development are regulated in the microsite is elevation [49]. A raster-formatted elevation map was produced using the DEM. According to the newly reclassified elevation map (Fig. 5b), soil erosion is a problem in 1.98 km^2 (0.06%) of the land use, 20.0 km^2 (0.66%), 56.76 km^2 (1.86%), 429.46 km^2 (14.04%), and 2550.13 km^2 (83.38%) of the land use (Table 5).

5.4. Impact of land use land cover on soil erosion

Percentage distribution of land use/cover and sensitive to erosion classes in Karnaphuli Watershed presented in Table 6. The reclassified land use map (Fig. 6b) indicated that 1788.124476 km^2 (58.48%) of the land use is very high sensitive; 609.398136 km^2 (19.93%) highly sensitive; 68.355363 km^2 (2.24%) moderate sensitive; 524.853011 km^2 (17.16%) low sensitive and 66.830426 km^2 (2.19%) very low sensitive to soil erosion.

5.5. Impact of SPI on soil erosion

It is calculated using map algebra and Equation (5) in the GIS environment utilizing the DEM data. According to the reclassified SPI map (Fig. 7b and Table 6), 142.47 km^2 (4.66%) of the area is very susceptible to soil erosion, followed by 596.51 km^2 (19.51%), 849.09 km^2 (27.76%), 323.33 km^2 (10.57%), low susceptible, and 1146.93 km^2 (37.5%).

5.6. Impact of curvature on erosion

The equation used to determine the curvature is a problematic terrain derivative, and it depends on the accuracy of the input data. The curvature tool determines the second value from the input surface cell-by-cell. Because profile curvature impacts the flow's acceleration and deceleration and, consequently, its erosional and depositional processes, it was employed in this study to correlate with other parameters. The curvature of the surface in the gradient's direction is measured by profile curvature. The data obtained using the Curvature tool can be better understood and interpreted by visualizing contours on a raster. The importance of profile curvature was demonstrated in (Table 6 and Fig. 8). According to the reclassified profile curvature map (Figs. 8b), 169.66 km2 (5.55%) of the study area's land use is very susceptible to soil erosion, followed by 733.29 km2 (23.98%), 1521.62 km2 (49.75%), 517.68 km2 (16.93%), low susceptible, and 116.08 km2 (3.79%).

5.7. Impact of soil type on erosion

Some soil characteristics that are linked to erosion can be used to evaluate the erodibility of a given soil [55]. Because stable soil aggregates can effectively withstand the pounding action of rain and may protect soils even when runoff occurs, soil loss is connected to both erosivity and erodibility as well as erosivity [56]. Based on K value, there are four different categories of soil erodibility: very high, high, moderate, and low [57]. These categories are: 0.35–0.45, 0.25–0.35, 0.25–0.35, and 0.2 [29]. Although extremely fine sand and silt levels are favourably connected with soil loss, clay content is adversely correlated with soil loss [58,59]. The soil properties for soil erosion simulations are given in Table 8.

5.8. Impact of TWI on erosion

The TWI predicts soil depth and the steady-state moisture index, making it a surface parameter for measuring soil erosion [60]. According to the TWI map that has been reclassified (Fig. 10 and Table 5), 5.21 km^2 (0.17%) of the region is extremely sensitive, 37.88 km^2 (1.24%) is highly susceptible, 387 km^2 (12.66%) is medium susceptible, 1042 km^2 (34.08%) is low susceptible, and 1585 km^2 (51.85%) is highly susceptible. soil erosion prone to a great extent. The findings showed that regions with high erosion rates are connected to lower TWI. In the current study, higher levels of erosion can be linked to plant cover in regions with lower TWI.

5.9. Impact of rainfall on soil erosion

The magnitude of precipitation has a notable influence on the process of soil erosion, contingent upon factors such as the specific type of precipitation, its duration, and the degree of intensity experienced within a given season or year [61]. The spatial distribution of annual rainfall map is classified into five classes such as (4208.59–4277.59) mm/year, (4277.59–4346.59) mm/year, (4346.59–4415.59) mm/year, (4415.59–4484.59) mm/year and (4484.59–4553.59) mm/year (Fig. 11).

5.10. Mapping of soil erosion susceptibility (SES)

Based on the methodology designed to map the soil erosion hot spots, all selected factors were superimposed to map the area susceptible to erosion as very high, high, medium, low, and very low. Allowing to the overall suitability score directed as; 0.0888km2 (0.003%), 137.8921km2 (4.561%), 1249.655km2 (41.339%), 1618.627km2 (53.545%) and 16.694 km2 (0.552%) areas are very high, high, medium, low and very low prone to soil erosion respectively (Fig. 12; Table 9). The highly susceptible soil erosion areas were concentrated mainly in the east and west parts of the basin. Based on this result, it is important to facilitate planning and involvement to reduce soil erosion problems in the watershed. Therefore, this study has designed a roadmap for multi-criteria decision-makers to bring sustainable development into the study area development into the study area.

5.11. Validation of potential soil erosion risk

Accuracy assessment/validation is an essential part of any mapping project. However, there is yet to be a specific method that can validate the soil vulnerability mapping strategy. Despite this, the location-based vulnerability maps were evaluated using a qualitative validation approach [64]. Personal observation, expertise opinions, and previous records were employed to assess the accuracy of soil erosion susceptibility mapping. Besides, 100 randomly located points in the study area as ground truth data to visually validate the produced soil erosion susceptibility map (Fig. 13).

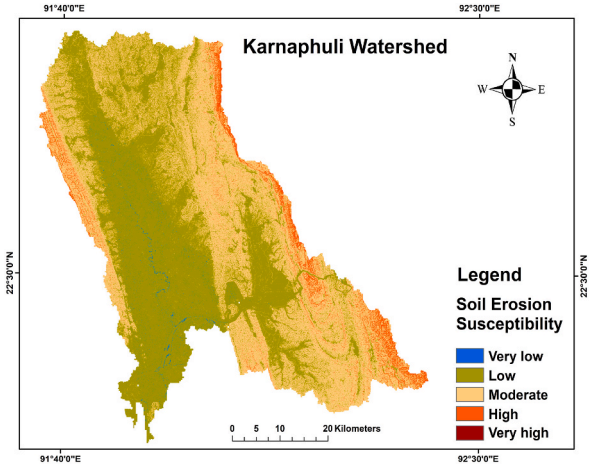

Fig. 12. Soil erosion severity map of the Karnaphuli river basin.

Table 9
Area under the risk of soil erosion.

No.	Area in Sq. km	Area (%)	Risk
1	16.693	0.552	Very low
2	1618.626	53.544	Low
3	1249.654	41.339	Moderate
4	137.891	4.561	High
5	0.088	0.003	Very high

6. Conclusion

In this study, the AHP technique integrated within the GIS environment was utilized to map potential erosion, its spatial pattern, and the influence of several parameters in the Karnaphuli watershed located in the district Chattogram of Bangladesh. The prime objective of the erosion risk map was to map erosion soil hotspot areas in the Karnaphuli watershed which was created by taking into account seven significant factors, including slope, stream power index, topographic wetness index, elevation, soil, curvature, and land use land cover.

There are several techniques to enhance the evaluation of water and soil resources with the help of GIS and the analytical hierarchy process (AHP). In order to improve the prioritizing of watershed regions for better management decisions, this research integrated a qualitative approach with AHP and GIS tools for mapping erosion potential. As a result of this concept, watershed managers now have a simple way to map erosion potential and prioritize control zones, which will help them allocate resources more effectively and efficiently for watershed management. According to the AHP results, slope, elevation, LULC, and SPI are highly important, indicating that the land area is vulnerable to soil erosion. This method resulted in a map that displayed major regions of probable erosion. The results show that slope is essential to degradation and soil erosion. Numerical weights are assigned to each parameter according to the hierarchy of each factor. Due to a lack of resources and a limited timescale, land use, and land cover classification accuracy was accomplished by obtaining reference points from Google Earth images instead of the field survey.

The research findings can help planners and policymakers make proper water and soil conservation decisions to reduce the problems of soil loss and depletion in the catchment area. Moreover, GIS and AHP of spatial susceptibility of soil loss can help to determine whether the soil conservation plan should be prioritized.

CRediT authorship contribution statement

Rubaiya Zumara: Writing – review & editing, Writing – original draft, Visualization, Software, Methodology, Investigation, Formal analysis, Data curation, Conceptualization. **N M Refat Nasher:** Writing – review & editing, Supervision.

Declaration of competing interest

The authors declare that they have no known competing financial interests or personal relationships that could have appeared to influence the work reported in this paper.

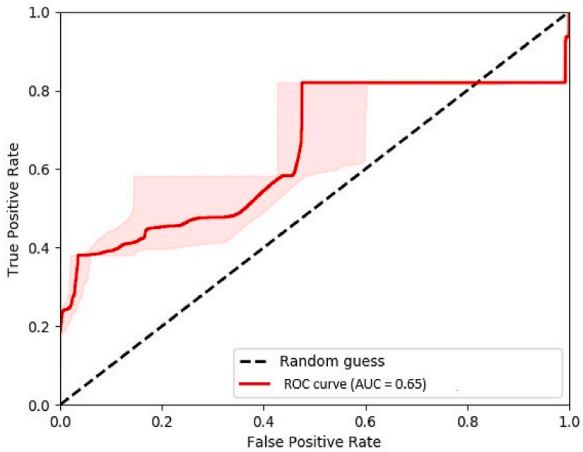

Fig. 13. ROC curve for validation of soil erosion potential risk.

Acknowledgements

We would like to express our sincere gratitude to the editors considering our manuscript for publication. We extended our heartfelt appreciation to the anonymous reviewers for their insightful feedback and constructive comments have played a crucial role improving the quality and rigor of our work. Additionally, we would like to thank the USGS, NASA, and FAO for providing free access to topographic, meteorological, and soil data sites.

References

[1] J. Boardman, J. Poesen, M. Evans, Slopes: soil erosion, Geological Society, London, Memoirs 58 (1) (2022) 241–255.
[2] P. Borrelli, et al., Land use and climate change impacts on global soil erosion by water (2015-2070), Proc. Natl. Acad. Sci. USA 117 (36) (2020) 21994–22001.
[3] M.J. Hann, R.P.C. Morgan, Evaluating erosion control measures for biorestoration between the time of soil reinstatement and vegetation establishment, Earth Surf. Process. Landforms: The Journal of the British Geomorphological Research Group 31 (5) (2006) 589–597.
[4] A. Halefom, A. Teshome, Modelling and mapping of erosion potentiality watersheds using AHP and GIS technique: a case study of Alamata Watershed, South Tigray, Ethiopia, Modeling Earth Systems and Environment 5 (3) (2019) 819–831.
[5] M. Khosrokhani, B. Pradhan, Spatio-temporal assessment of soil erosion at Kuala Lumpur metropolitan city using remote sensing data and GIS, Geomatics, Nat. Hazards Risk 5 (3) (2014) 252–270.
[6] M.N. Jebur, B. Pradhan, M.S. Tehrany, Optimization of landslide conditioning factors using very high-resolution airborne laser scanning (LiDAR) data at catchment scale, Remote Sensing of Environment 152 (2014) 150–165.
[7] S.A. El-Swaify, Factors affecting soil erosion hazards and conservation needs for tropical steeplands, Soil Technol. 11 (1) (1997) 3–16.
[8] G. Bove, A. Becker, B. Sweeney, M. Vousdoukas, S. Kulp, A method for regional estimation of climate change exposure of coastal infrastructure: case of USVI and the influence of digital elevation models on assessments, Sci. Total Environ. 710 (2020) 136162.
[9] S.R. Rogers, I. Manning, W. Livingstone, Comparing the spatial accuracy of digital surface models from four unoccupied aerial systems: photogrammetry versus LiDAR, Rem. Sens. 12 (17) (2020) 2806.
[10] P.R. Tribhuvan, M.A. Sonar, Morphometric analysis of a Phulambri river drainage basin (Gp8 Watershed), Aurangabad district (Maharashtra) using geographical information system, International Journal of Advanced Remote Sensing and GIS 5 (6) (2016) 1813–1828.
[11] M.R. Rahman, Impact of riverbank erosion hazard in the Jamuna floodplain areas in Bangladesh, Journal of Science Foundation 8 (1–2) (2010) 55–65.
[12] J.R. Comino, et al., Quantitative comparison of initial soil erosion processes and runoff generation in Spanish and German vineyards, Sci. Total Environ. 565 (2016) 1165–1174.
[13] J.M. Garcia-Ruiz, S. Beguería, E. Nadal-Romero, J.C. González-Hidalgo, N. Lana-Renault, Y. Sanjuán, A meta-analysis of soil erosion rates across the world, Geomorphology 239 (2015) 160–173.
[14] S. Karmakar, S.M. Sirajul Haque, M. Mozaffar Hossain, M. Shafiq, Water quality of Kaptai reservoir in chittagong hill tracts of Bangladesh, J. For. Res. 22 (2011) 87–92.
[15] S.K. Roy, U.K. Navera, MORPHOLOGICAL RESPONSES OF A TIDAL RIVER DUE TO CLIMATE CHANGE: A CASE STUDY FOR KARNAFULI RIVER, BANGLADESH, 2018.
[16] M. López-Vicente, S. Álvarez, Influence of DEM resolution on modelling hydrological connectivity in a complex agricultural catchment with woody crops, Earth Surf. Process. Landforms 43 (7) (2018) 1403–1415.
[17] H. Zhao, et al., Extraction of terraces on the Loess Plateau from high-resolution DEMs and imagery utilizing object-based image analysis, ISPRS Int. J. Geo-Inf. 6 (6) (2017) 157.
[18] R. Ahammad, M.K. Hossain, I. Sobhan, R. Hasan, S.R. Biswas, S.A. Mukul, Social-ecological and institutional factors affecting forest and landscape restoration in the Chittagong Hill Tracts of Bangladesh, Land Use Pol. 125 (2023) 106478.
[19] B.A. Al Shoumik, M.Z. Khan, M.S. Islam, Soil Erosion Estimation by RUSLE Model Using GIS and Remote Sensing Techniques: A Case Study of the Tertiary Hilly Regions in Bangladesh from 2017 to 2021, 2023.
[20] A. Gafur, J.R. Jensen, O.K. Borggaard, L. Petersen, Runoff and losses of soil and nutrients from small watersheds under shifting cultivation (Jhum) in the Chittagong Hill Tracts of Bangladesh, J. Hydrol. 274 (1) (2003) 30–46, https://doi.org/10.1016/S0022-1694(02)00351-7.
[21] F. Hossain, A.M. Kamal, S. Sadeak, M.Y. Gazi, Quantitative soil erosion risk assessment due to rapid urbanization in the Cox's Bazar district and Rohingya refugee camps in Bangladesh, Stoch. Environ. Res. Risk Assess. 37 (3) (2023) 989–1006.
[22] T. Ahmed, S. Alam, M.S. Hasan, Modeling climate change impact on hydrology of Karnafuli River basin using soil water assessment tool (SWAT), in: 4th International Conference on Water and Flood Management (ICWFM-2013), 2013, pp. 529–536. Dhaka.
[23] S.N.H. Rizvi, Bangladesh District Gazetteers: Chittagong, East Pakistan Government Press, Dhaka, 1975.
[24] R.J. Lara, S.B. Neogi, M.S. Islam, Z.H. Mahmud, S. Yamasaki, G.B. Nair, Influence of catastrophic climatic events and human waste on Vibrio distribution in the Karnaphuli estuary, Bangladesh, EcoHealth 6 (2009) 279–286.
[25] M.W. Alam, M. Zafar, Occurrences of Salmonella spp. in water and soil sample of the Karnafuli river estuary, Microb. Health 1 (2) (2012) 41–45.
[26] A. Mosavi, F. Sajedi-Hosseini, B. Choubin, F. Taromideh, G. Rahi, A.A. Dineva, Susceptibility mapping of soil water erosion using machine learning models, Water 12 (7) (2020), 1995.
[27] C.K. Wentworth, A simplified method of determining the average slope of land surfaces, Am. J. Sci. 5 (117) (1930) 184–194.
[28] S. Saha, A. Gayen, H.R. Pourghasemi, J.P. Tiefenbacher, Identification of Soil Erosion-Susceptible Areas Using Fuzzy Logic and Analytical Hierarchy Process Modeling in an Agricultural Watershed of Burdwan District, India, vol. 78, Environmental Earth Sciences, 2019, pp. 1–18.
[29] J.R. Anderson, Land-use Classification Schemes, Photogrammetric Engineering, 1971.
[30] C.-Y. Chen, F.-C. Yu, Morphometric analysis of debris flows and their source areas using GIS, Geomorphology 129 (3–4) (2011) 387–397.
[31] L.W. Zevenbergen, C.R. Thorne, Quantitative analysis of land surface topography, Earth Surf. Process. Landforms 12 (1) (1987) 47–56.
[32] T.M. Pavelsky, L.C. Smith, RivWidth: a software tool for the calculation of river widths from remotely sensed imagery, Geosci. Rem. Sens. Lett. IEEE 5 (1) (2008) 70–73.
[33] C.-Z. Qin, et al., An approach to computing topographic wetness index based on maximum downslope gradient, Precis. Agric. 12 (2011) 32–43.
[34] N.C. Wijesundara, N.S. Abeysingha, D. Dissanayake, GIS-based soil loss estimation using RUSLE model: a case of Kirindi Oya river basin, Sri Lanka, Modeling Earth Systems and Environment 4 (2018) 251–262.
[35] S. Arekhi, Y. Niazi, A.M. Kalteh, Soil erosion and sediment yield modeling using RS and GIS techniques: a case study, Iran, Arabian J. Geosci. 5 (2) (2012) 285.
[36] D. Asteriou, S.G. Hall, ARIMA models and the Box–Jenkins methodology, Applied Econometrics 2 (2) (2011) 265–286.
[37] T.L. Saaty, "The analytic hierarchy process mcgraw hill, New York,", Agric. Econ. Rev. 70 (1980).
[38] G.S. Bhunia, S. Samanta, B. Pal, Quantitative analysis of relief characteristics using space technology, Int. J. Phys. Soc. Sci. 2 (8) (2012) 350–365.
[39] N. Mhazo, P. Chivenge, V. Chaplot, Tillage impact on soil erosion by water: discrepancies due to climate and soil characteristics, Agric. Ecosyst. Environ. 230 (2016) 231–241.
[40] D.F. Ritter, R.C. Kochel, J.R. Miller, J.R. Miller, *Process Geomorphology*, No. 551.4 R5. Wm. C. Brown Dubuque, 1995. Iowa.
[41] J.K. Weissel, L.F. Pratson, A. Malinverno, The length-scaling properties of topography, J. Geophys. Res. Solid Earth 99 (B7) (1994) 13997–14012.
[42] S.K. Garg, Geology: the Science of Earth, Khanna, 1991.
[43] A.N. Strahler, Hypsometric (area-altitude) analysis of erosional topography, Geol. Soc. Am. Bull. 63 (11) (1952) 1117–1142.

[44] M.P. Bishop, J.F. Shroder Jr., R. Bonk, J. Olsenholler, Geomorphic change in high mountains: a western Himalayan perspective, Global Planet. Change 32 (4) (2002) 311–329.
[45] S.S. Saini, R. Jangra, S.P. Kaushik, Vulnerability assessment of soil erosion using geospatial techniques-A pilot study of upper catchment of Markanda river, International journal of advancement in remote sensing, gis and geography 2 (1) (2015) 9–21.
[46] N. Tahmassebipoor, O. Rahmati, F. Noormohamadi, S. Lee, Spatial analysis of groundwater potential using weights-of-evidence and evidential belief function models and remote sensing, Arabian J. Geosci. 9 (2016) 1–18.
[47] R. Zakerinejad, M. Maerker, An integrated assessment of soil erosion dynamics with special emphasis on gully erosion in the Mazayjan basin, southwestern Iran, Nat. Hazards 79 (Suppl 1) (2015) 25–50.
[48] L. Lombardo, P.M. Mai, Presenting logistic regression-based landslide susceptibility results, Eng. Geol. 244 (2018) 14–24.
[49] F.S. Chapin, A.J. Bloom, C.B. Field, R.H. Waring, Plant responses to multiple environmental factors, Bioscience 37 (1) (1987) 49–57.
[50] C. Yilmaz, T. Topal, M.L. Süzen, GIS-based landslide susceptibility mapping using bivariate statistical analysis in Devrek (Zonguldak-Turkey), Environ. Earth Sci. 65 (2012) 2161–2178.
[51] H. Blanco, R. Lal, Principles of Soil Conservation and Management, vol. 167169, Springer, New York, 2008.
[52] C. Gokceoglu, H. Sonmez, H.A. Nefeslioglu, T.Y. Duman, T. Can, The 17 March 2005 Kuzulu landslide (Sivas, Turkey) and landslide-susceptibility map of its near vicinity, Eng. Geol. 81 (1) (2005) 65–83.
[53] B. Fu, L. Chen, Agricultural landscape spatial pattern analysis in the semi-arid hill area of the Loess Plateau, China, J. Arid Environ. 44 (3) (2000) 291–303.
[54] A.W. Western, R.B. Grayson, The Tarrawarra data set: soil moisture patterns, soil characteristics, and hydrological flux measurements, Water Resour. Res. 34 (10) (1998) 2765–2768.
[55] S. Stanchi, M. Freppaz, D. Godone, E. Zanini, Assessing the susceptibility of alpine soils to erosion using soil physical and site indicators, Soil Use Manag. 29 (4) (2013) 586–596.
[56] T.J. Toy, G.R. Foster, K.G. Renard, Soil Erosion: Processes, Prediction, Measurement, and Control, John Wiley & Sons, 2002.
[57] G.T. Amangabara, N. Chukwuocha, C. Amaechi, Determination of the erodibility status of some soils in Ikeduru Local Government area of IMO State, Nigeria, International Journal of Geology 4 (1) (2014) 240–246.
[58] S.W. Duiker, D.C. Flanagan, R. Lal, Erodibility and infiltration characteristics of five major soils of southwest Spain, Catena 45 (2) (2001) 103–121.
[59] W.H. Wischmeier, D.D. Smith, Predicting Rainfall Erosion Losses: a Guide to Conservation Planning, vol. 537, Department of Agriculture, Science and Education Administration, 1978.
[60] P.E. Gessler, I.D. Moore, N.J. McKenzie, P.J. Ryan, Soil-landscape modelling and spatial prediction of soil attributes, Int. J. Geogr. Inf. Syst. 9 (4) (1995) 421–432.
[61] Q. Yang, Y. Xie, W. Li, Z. Jiang, H. Li, X. Qin, Assessing soil erosion risk in karst area using fuzzy modeling and method of the analytical hierarchy process, Environ. Earth Sci. 71 (2014) 287–292.